Transactions of the Korean Society of Mechanical Engineers. Vol. 6, No. 3, pp. 271~281, 1982. 271

<Original>

# A Study on the Prediction of the Limiting Depth of Cut in Dynamic Cutting of a Tapered Workpiece

**J.B. Ssengonzi*, Jang Moo Lee** and Young Ha Yum**.**

(Received March 10, 1982)

# 테이퍼진 가공물의 동적 한계절삭깊이의 예측에 관한 연구

쌩 곤 지·이 장 무·염 영 하


## 초 록

이 연구는 테이퍼진 가공물이 동적 절삭상태에서 가지는 한계절삭깊이의 예측을 위한 이론 및 실험적 방법을 논하였다. 절삭 모델은 Usui-Hirota(1)가 제안한 것을, 가공물의 형상은 MTIRA(2)가 제안한 공작기계 동적성능시험용 표준시편을 다소 수정하여 사용하였다. 칩유동각은 Usui-Hirota의 에너지 방법에 의하여 구하였고, Inamura-Sata(6)의 원통형 가공물에 대한 절삭동력학 이론을 일반화시켜 테이퍼진 가공물에 적용하여 절삭의 안정한계를 구한 후 채터시험 결과와 비교하여 이론의 타당성을 검증하였다.


## Nomenclature

- $A$ : Total shear surface area
- $C$ : Equivalent damping coefficient
- $C_e$ : End cutting edge angle
- $C_s$ : Side cutting edge angle
- $D$ : Universal machinability index
- $D'$ : Effective undeformed chip thickness
- $\mathcal{D}$ : Depth factor
- $dB$ : Width of cut of an element
- $f$ : Frequency
- $F$ : Feed
- $i$ : Inclination angle of side cutting edge
- $j$ : $\sqrt{-1}$
- $K_t$ : Equivalent spring constant
- $K_c$ : Main cutting stress
- $K_s$ : Shear stress
- $m$ : Equivalent mass
- $Q$ : Projected cutting cross-section area on tool face in cutting direction
- $Q'$ : Cutting cross-section area defined on basic plane
- $R$ : Tool nose radius
- $V$ : Cutting velocity
- $V_c$ : Chip-flow velocity
- $V$-$V_c$ : Cutting plane
- $X_t$ : Amplitude of tool oscillation normal to cut surface
- $X_t'$ : Amplitude of inner modulation
- $X_t''$ : Amplitude of outer modulation
- $\alpha_n$ : Normal rake angle
- $\alpha_e$ : Effective rake angle
- $\beta$ : Friction angle
- $\phi$ : Shear angle
- $\psi$ : Angular coordinate of point on tool nose
- $\zeta$ : Taper angle
- $\eta_c$ : Chip-flow angle

* Seoul National Univ.
** Member, Seoul National Univ.

$\eta_c'$ : Projected chip-flow angle

$\epsilon$ : Phase shift between inner and outer modulation

## 1. Introduction

Dynamic performance of machine tool can be evaluated in two ways. One is direct cutting test proposed by MTIRA(2)(Machine Tool Industrial Research Association, England), which is basically a technique of design of experiment(a statistical and experimental approach). The tests are performed with standard workpiece specimens of varying depth of cut, i.e., tapered workpieces under various cutting conditions. The limiting depth of cut of that tapered workpiece can be used to compare the dynamic performance of machine tools. The other is indirect excitation test which has been employed by many researchers(3, 4, 5, 6) to understand and predict the dynamic behavior of machine tools. In this test, structural dynamics of a machine tool with a cylindrical workpiece is identified under a certain cutting condition(7). Then the limiting depth of cut can be predicted by utilizing the analytically derived cutting dynamics and the experimentally obtained structural dynamics and steady state cutting data. However, there have not been any attempts to link or correlate both test results so far. It is thus the purpose of this study that the theory of cutting dynamics and chatter can be established for the machine tool with the tapered workpiece to link the two methods and the theory will be effectively utilized to improve the dynamic performance of machine tools.

## 2. Three Dimensional Static Cutting Model

A two dimensional interpretation of three dimensional cutting process may be found in reference(1). When this interpretation is applied to a tapered specimen, a number of cases for the cutting cross-section are observed. In this report a detailed derivation of expressions for

i) effective undeformed chip thickness,

ii) shear surface area,

iii) projected area of cutting cross-section.

is omitted.

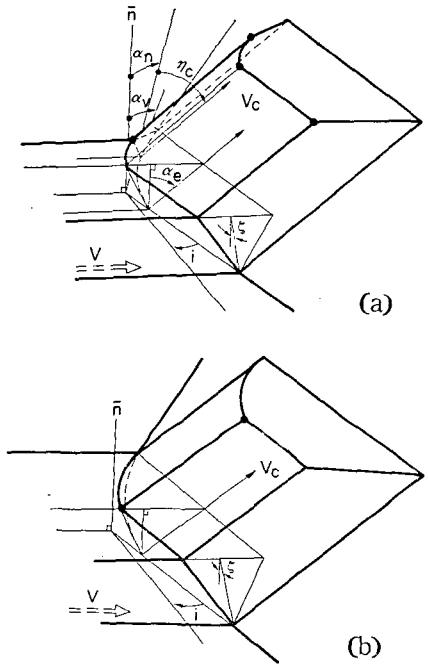


Fig. 1 The static cutting model.

## 3. Prediction of Chip Flow Angle

It is known that the effective rake angle, in three dimensional cutting, plays the same role as the normal rake angle in two dimensional cutting. The effective rake angle $\alpha_e$ is the angle between a plane perpendicular to the cutting speed vector and a tangent to the tool face drawn in the direction of chip flow. Its value is obtained from the geometrical constitution as:

$$\alpha_e=\sin^{-1}(\sin\alpha_n\cos i\cos\eta_c+\sin\eta_c\sin i) \quad (1)$$

where $\eta_c$ : chip flow angle

$\alpha_n$ : normal rake angle

$i$ : cutting edge inclination angle

When the side cutting edge is rotated through the side cutting edge angle it occupies the position shown by the dotted lines in the figure below. Cutting forces $F_H'$, $F_V'$, $F_T'$ for the situation so obtained are calcutated first and a conversion to $F_V, F_H, F_T$ is made by:

$$\begin{aligned} F_H&=F_H' \\ F_V&=F_V'\cos C_S-F_T'\sin C_S \\ F_T&=F_T\cos C_S+F_V'\sin C_S \end{aligned} \quad (2)$$

It is assumed that cutting energy is consumed as energy of shear, required to create the shear surface and friction energy, ($U_f$), of the chip on the tool face. The tool is considered very sharp and friction processes at the flank can be neglected. Then the shear energy, $U_s$, and friction energy are calculated from:

$$\begin{aligned} U_s&=F_sV_s=\frac{\tau_s\cos\alpha_e}{\cos(\phi_e-\alpha_e)}\cdot A.V \\ U_f&=F_tV_c=\frac{\tau_s\sin\beta\cos\alpha_e}{\cos(\phi_e-\beta-\alpha')}\cdot \\ &\qquad \frac{1}{\cos(\phi_e-\alpha_e)}\cdot Q.V \end{aligned} \quad (3)$$

where A is the total area of shear surface, $Q$ is the projected area of the cutting crosssection to the tool face in the direction of cutting velocity $V$, $\phi_e$ is the effective shear angle, $\tau_s$ shear stress, and $\beta$ friction angle. The energy approach assumes that chip flows in such a direction specified by chip flow angle($\eta_c$)

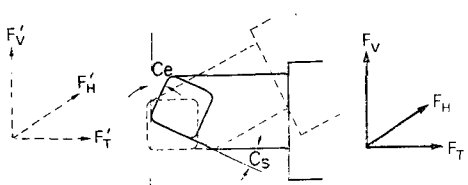


**Fig. 2** Rotation of the main cutting edge.

which minimizes the total cutting energy, thus

$$U=U(\eta_c)=(U_s+U_f)_{min} \quad (4)$$

The following assumptions have been shown to agree with experimental observations:

The relationships between $\phi_e, \tau_s, \beta$ and $\alpha_e$ for three dimensional cutting are the same as the relationships between $\phi, \tau_s, \beta$ and $\alpha_n$ for orthogonal cutting.

Therefore empirical relations such as Eqs. (5), (6) and (7) may be derived from steady state orthogonal cutting experiments.

$$\phi_e=f(\alpha_e)=f(\alpha_n) \quad (5)$$

$$\tau_s=g(\alpha_e)=g(\alpha_n) \quad (6)$$

$$\beta=h(\alpha_e)=h(\alpha_n) \quad (7)$$

When turning a tapered workpiece the shape of the cutting cross-section depends on tool geometry, cutting parameters, and taper angle $\zeta$ of the workpiece.

In the case $R\geqq F\cos C_s/\{1+\sin(C_e-C_s)\}$ four cutting cross-sections are illustrated in Fig. 3. Expressions for the shear surface area and the projected area of the cutting cross-sections are also given.

For the case $R<F\cos C_s/\{1+\sin(C_e-C_s)\}$ there are three more cutting cross-sections, which are not illustrated, for simplicity in this report.

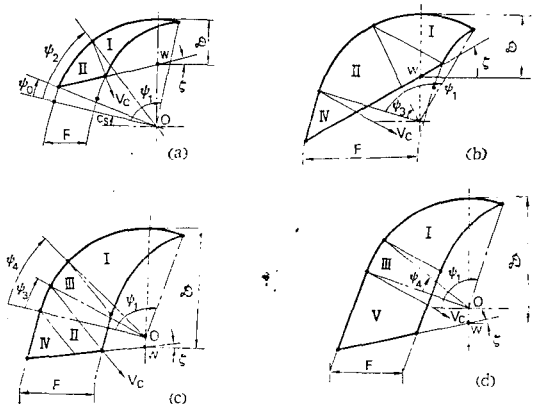


**Fig. 3** Cutting cross-sections.

## 4. Shear Plane and Projected Area

i) For the case when $R-\mathfrak{D}\geqq R\sin(\zeta+C_s)/\cos\zeta$.

The area of the shear surface, $A$, is given

by

$$A=\int_{\phi_2}^{\phi_1} f_I(\psi)ds+\int_{\phi_0}^{\phi_2} f_{II}(\psi)ds \tag{8}$$

where:

$$f_I(\psi)=\{F+R\cos(\psi+C_s)\}\left[\sin(\eta_c'+C_s)\cdot\cot\left\{\tan^{-1}\left(\frac{F+R\cos(\psi+C_s)}{R\sin(\psi+C_s)}\right)\right\}+\cos(\eta_c'+C_s)\right]-\left[R^2-\left[\{F+R\cos(\psi+C_s)\}\left[\sin(\eta_c'+C_s)-\cos(\eta_c'+C_s)\times\cot\left\{\tan^{-1}\left(\frac{F+R\cos(\psi+C_s)}{R\sin(\psi+C_s)}\right)\right\}\right]\right]^2\right]^{1/2} \tag{9}$$

$$f_{II}(\psi)=R\cos(\eta_c'\psi)-\frac{\cos\zeta(R-\mathcal{D})}{\sin(\zeta+\eta_c'+C_s)}-R\frac{\sin(\eta_c'-\psi)}{\tan(\eta_c'+C_s+\zeta)} \tag{10}$$

$$ds=\frac{R}{\sin\phi_e}\left[\cos^2(\eta_c'-\psi)+\left\{\cos\phi_e\sin(\eta_c'-\psi)+\frac{\sin\phi_e}{\cos i}\left\{\sin i\cos\psi-\tan\alpha_n(\sin^2 i+1)\sin\psi\right\}\right\}^2\right]^{1/2}d\psi \tag{11}$$

$$\phi_0=\sin^{-1}\left[\left(\frac{R-\mathcal{D}}{R}\right)\cos\zeta\right]-(C_s+\zeta) \tag{12}$$

$$\phi_1=\frac{\pi}{2}-C_s+\tan^{-1}\left(\frac{F}{\sqrt{(4R^2-F^2)}}\right) \tag{13}$$

$$\phi_2=\eta_c'-\sin^{-1}\left\{\frac{1}{R}\sqrt{y^2+(\sqrt{R^2-Y^2}-F)^2}\times\sin[\eta_c'+C_s-\tan^{-1}(y/(\sqrt{R^2-y^2}-F))]\right\} \tag{14}$$

$$y=\frac{1}{1+\tan^2\zeta}\left[(F\tan\zeta-L)-\tan\zeta\sqrt{R^2(1+\tan^2\zeta)-(F\tan\zeta-L)^2}\right] \tag{15}$$

$$L=\mathcal{D}-R \tag{16}$$

where $\mathcal{D}$ is the depth factor and $R$ is the tool nose radius.

The projected area $Q$ is given by: $Q'/\cos\alpha_n \cos i$ where $Q'$ is the cutting cross-section area given by:

$$Q'=\{R^2\tan^{-1}(F/(\sqrt{4R^2-F^2}))+0.25F\sqrt{4R^2-F^2}-Fy\}+0.5F[y-R\sin\{\sin^{-1}[\cos\zeta(R-\mathcal{D})/R]-\zeta] \tag{17}$$

ii) For the case when $R-\mathcal{D}<\frac{R\sin(\zeta+C_s)}{\cos\zeta}$ and $\mathcal{D}\leq F\tan\zeta+R-R(\cos C_s\tan\zeta+\sin C_s)$. The shear area $A$ is calculated from:

$$A=\int_{\phi_2}^{\phi_1} f_I(\psi)ds+\int_0^{\phi_2} f_{II}(\psi)ds+A_N \tag{18}$$

$$A_N=\frac{A'[\cos^2\alpha_e-\sin^2\phi_e\{\sin\eta_c-(\sin\alpha_e\cos i\cos\alpha_e\cos\eta_c'+\cos\alpha_e\cot\phi_e)\sin i\}^2]^{1/2}}{\sin\phi_e} \tag{19}$$

$$A'=\frac{0.5\cos\eta_c'[R\sin(C_s+\zeta)+(\mathcal{D}-R)\cos\zeta]}{\cos(C_s+\zeta)\sin(\zeta+\eta_s'+C_s)}\cdot[R\sin(C_s+\zeta)+(\mathcal{D}-R)\cos\zeta] \tag{20}$$

The cutting cross-section area $Q'$ a is calculated from:

$$Q'=A'+F(y-R\sin C_s)-0.5(y-R\sin C_s)\left\{\frac{(R-\mathcal{D})-R\sin C_s}{\tan\zeta}+(F-R\cos C_s)\right\}+\frac{0.5\sin(\eta_c'+C_s)}{\sin\zeta\sin(\eta_c'+C_s+\zeta)}\left[R\sin(\zeta+C_s)+(\mathcal{D}-R)\cos\zeta\right]^2+R^2\tan^{-1}(F/\sqrt{(4R^2-F^2)})+0.25F\sqrt{(4R^2-F^2}-Fy \tag{21}$$

iii) For the case when $F\tan\zeta+R-R(\cos C_s\tan\zeta+\sin C_s)<\mathcal{D}$ Fig. 3c.

and

$$\mathcal{D}\geq\frac{1}{\tan C_s}\left[\frac{R\cos(C_s+\zeta)}{\cos\zeta}-F\frac{\cos(\eta_c'+C_s)\cos(C_s+\zeta)}{\cos\eta_c'\cos\zeta}+F\right]+R-R/\sin C_s$$

we have

$$A=\int_{\phi_4}^{\phi_1} f_I(\psi)ds+\int_{\phi_3}^{\phi_4} f_{III}(\psi)ds+\int_0^{\phi_3} f_{II}(\psi)ds+A_N \tag{22}$$

where

$$f_{III}(\psi)=\frac{1}{\sin(\eta_c'+C_s)}\left\{R\sin(\psi+C_s)-\frac{R\sin(\eta_c'+C_s)-F\sin(\eta_c'+C_s)\cos}{\cos}\frac{C_s-R\sin(\eta_c'-\psi)\cos C_s}{\eta_c'}\right\} \tag{23}$$

$$\psi_3=\eta_c'+\sin^{-1}\left[\frac{1}{R}\left\{F\sin(\eta_c'+C_s)-R\left\{\frac{\sin(\eta_c'+C_s)-\cos\eta_c'}{\cos C_s}\right\}\right.\right.$$

$$-\frac{\cos\eta_c'}{\cos C_s}\left\{\left[\frac{R+L\sin C_s-F\cos C_s}{\cos(C_s+\zeta)}\right]\sin\zeta+\mathcal{D}\right\}\Big]\Big] \quad (24)$$

The projected area $Q$ is given by

$$Q=Q'/\cos\alpha_n\cos i$$

where $Q'$ is the cutting cross-section area given by:

$$Q'=A''+R^2\tan^{-1}(F/(\sqrt{4R^2-F^2}))+0.25F\sqrt{4R^2-F^2}-FR\sin C_s \quad (25)$$

$$A''=0.5F\cos C_s\left\{\frac{R\sin(C_s-\zeta)+L\cos\zeta}{\cos(C_s+\zeta)}+\left[\frac{R+L\sin C_s-F\cos C_s}{\cos(C_s+\zeta)}\right]\frac{\sin\zeta}{\cos C_s}+R\sin C_s/\cos C_s+L/\cos C_s\right\} \quad (26)$$

iv) For the case when

$$\mathcal{D}>\frac{1}{\tan C_s}\left[\frac{R\cos(C_s+\zeta)}{\cos\zeta}-\frac{F\cos(\eta_c'+C_s)\cos(C_s+\zeta)}{\cos\eta_c'\cos\zeta}+F\right]+R-R/\sin C_s$$

we have:

$$A=\int_{\phi_4}^{\phi_1}f_{\mathrm{I}}(\phi)ds+\int_0^{\phi_4}f_{\mathrm{II}}(\phi)ds+A_{\mathrm{V}} \quad (27)$$

$$A_{\mathrm{V}}=A_{\mathrm{V}}'\frac{[\cos^2\alpha_e-\sin^2\phi_e\{\sin\eta_c-(\sin\alpha_e+\cos\alpha_e\cot\phi_e)\sin i\}^2]^{1/2}}{\cos i\cos\alpha_e\cos\eta_c'\sin\phi_e} \quad (28)$$

$$A_{\mathrm{V}}'=0.5F[2\{\mathcal{D}''-R(1-\sin C_s)\}-F\cos^2C_s\tan\eta_c'-F\sin C_s\cos C_s]-0.5F^2\cos C_s\sin\zeta/\cos(C_s+\zeta)$$

$$Q=\frac{1}{\cos i\cos\alpha_n}\left\{R^2\tan^{-1}\left(\frac{F}{\sqrt{4R^2-F^2}}\right)+0.25F\sqrt{4R^2-F^2}+F(\mathcal{D}''-R)-0.5\frac{F^2\cos C_s\sin\zeta}{\cos(\zeta+C_s)}\right. \quad (29)$$

$$\mathcal{D}''=\mathcal{D}+\left[\frac{(R+L\sin C_s)}{\cos(C_s+\zeta)}\sin\zeta\right] \quad (30)$$

$$\phi_4=\eta_c'-\sin^{-1}\left\{\sin\eta_c'-\frac{F}{R}\sin(\eta_c'+C_s)\right\} \quad (31)$$

## 5. Dynamic Cutting of a Tapered Specimen

The dynamic cutting model is illustrated in Fig. 4. The cutting geometry is characterized by the side cutting edge angle $C_s$, the end cutting edge angle $C_e$, the cutting edge inclination angle $i$, the normal rake $\alpha_n$, the depth factor $\mathcal{D}$, the feed rate $F$ and the amplitude of tool oscillation normal to the work surface $X_t$. For the usual feed rates encountered in turning operations, variation of chip flow direction during one revolution may be assumed negligiable. Analysing the dynamic orthogonal cutting process appearing in the sliced plane containing both the cutting velocity vector and the mean chip flow vector $V_c$ expressions for the cutting and thrust forces in the $V-V_c$ plane may be derived in a similar way to the case of a cylindrical specimen; the only difference lies in the respective expressions for the effective depth of cut for the possible cutting cross-sections. Therefore the cutting and thrust forces, $F_c'$ and $F_t'$ will be given by 32 and 33 with the necessary change in $D'$

$$F_c'=\frac{K_c}{\sin\phi_e}\left[e^{-j\epsilon}\int N_2\,dB+\left\{-\int N_1\,dB+j\frac{2\pi f}{V}\left(\frac{D\cos\phi_e-1}{D\sin\phi_e}\right)\int D'N_1dB\right\}\right]X_t \quad (32)$$

$$F_t'=\frac{K_c}{\sin\phi_e}\left[\left(\frac{D\cos\phi_e-1}{D\sin\phi_e}\right)e^{-j\epsilon}\int N_2\,dB+\left\{-\left(\frac{D\cos\phi_c-1}{D\sin\phi_e}\right)\int N_1\,dB-j\frac{2\pi f}{V}\int D'\,N_1\,dB\right\}\right]X_t \quad (33)$$

where

$K_c$ : main stress, $D=K_c/K_s$

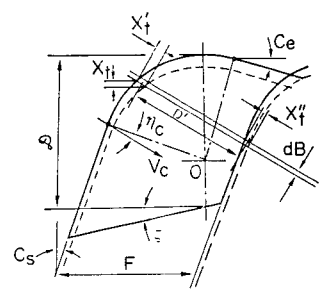


**Fig. 4** The dynamic cutting model.

$K_s$ : shear stress, $N_1=X_t'/X_t$

$f$ : frequency, $N_2=X_t''/X_t$

$D'$ : effective undeformed chip thickness

$dB$ : infinitesimal width of cut normal to $V-V_c$ plane

$\epsilon$ : phase shift between inner modulation $X_t'$ and outer modulation $X_t''$

## 6. The Resultant Cuttng Force

It is realized that the resultant cutting force ($\overline{F}$) in three dimensional cutting lies in the $V_c-F_{Res}$ plane determined by tool geometry while the vector($F'$), the vector sum of $F_c'$ and $F_t'$, lies in the $V-V_c$ plane. Resolve $F_{Res}$ into $F_r$ lying on the tool face and $F_n$ normal to it. Now the direction of $F_r$ is assumed to coincide with the direction of $V_c$. Then plane $V_c-F_{Res}$ is normal to the $V-V_c$ plane and $F_n$ may be further resolved into $F_n'$ lying on the $V-V_c$ plane and $N$ normal to it. See illustration below. Thus:

$$\overline{F}=\overline{F}_r+\overline{F}_n=\overline{F}_r+\overline{F}_n'+\overline{N}=\overline{F}_t'+\overline{F}_c'+\overline{N}=\overline{F}'+\overline{N} \quad (34)$$

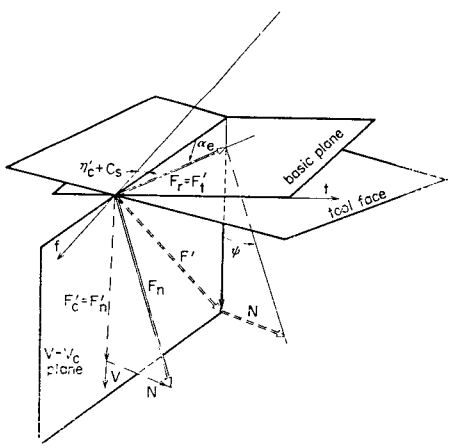


Fig. 5 The relation between $V-V_c$ and $V_c-F_{Res}$ planes.

## 7. Inner Modulation, Outer Modulation, Effective Undeformed Chip Thickness:

Dynamic cutting is considered as two processes which take place simultaneously. One is the wave cutting process represented by inner modulation and the other is the wave removing represented by outer modulation.

For convenience, inner modulation, outer modulation and the effective undeformed chip thickness are formulated as functions of a variable $p$. In the plane view of the cutting tool, set the origin of the x-y coordinate system to coincide with the centre of the tool nose as shown below. $p$, is the $y$ coordinate of a point $p$, the point of intersection of chipflow direction at any desired point $Q$ and the $y$ axis. From the figure, one may obtain:

i) for the points on the side cutting edge:

$$X_t'=X_t''=Q'T'=X_t\sin C_s/\cos\eta_c' \quad (35\text{-a})$$

ii) for the points on the end cutting edge:

$$X_t'=X_t''=Q''T''=X_t\cos C_e/\sin(\eta_c'+C_s-C_e) \quad (35\text{-b})$$

iii) for the points on the tool nose a nonlinear expression is obtained and linearlization we get:

$$X_t'=X_t''=[p\cos(\eta_c'+C_s)\cdot[E_1(p)]^{-1/2}+\sin(\eta_c'+C_s]X_t \quad (35\text{-c})$$

where

$$E_1(p)=R^2\sec^2(\eta_c'+C_s)-p^2$$

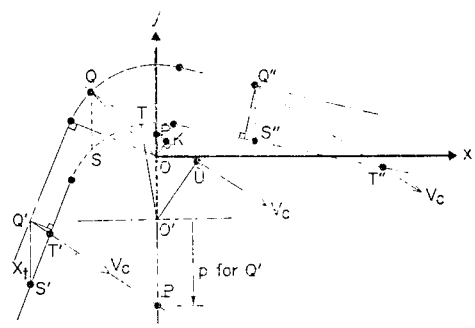


Fig. 6 The $p$ variable and the coordinate system.

$$\eta_c' = \tan^{-1}[(\tan\eta_c - \sin\alpha_n \tan i) \cos i/\cos\alpha_n] \quad (36)$$

Expressions for the effective undeformed chip thickness are listed below; $\zeta$ is the taper angle, $L=\mathcal{D}-R$:

i) when the side cutting edge removes stock from the original suface of the specimen

$$D_1'(p) = \left\{\frac{R+L\sin C_s}{\cos(C_s+\zeta)} + \frac{(p+L)\cos(\eta'_c{}'+C_s)}{\sin(\eta_c'+C_s+\zeta)}\right\}\frac{\cos(C_s+\zeta)}{\cos\eta_c'} \quad (37)$$

ii) when the end cutting edge removes chip from the original surface of the specimen

$$D_2'(p) = \frac{(p+L)\cos\zeta}{\sin(\eta_c'+C_s+\zeta)} - \frac{(p\cos C_e - R)}{\sin(\eta_c'+C_s-C_e)} \quad (38)$$

iii) when the tool nose is removing chip from the original surface of the specimen

$$D_3'(p) = [R^2-\{p\cos(\eta_c'+C_s)\}^2]^{1/2} + \frac{p[1+\cos 2(\eta_c'+C_s)] - p\sin 2(\eta_c'+C_s)\sin\zeta + 2L\cos\zeta}{2\sin(\eta_c'+C_s+\zeta)} \quad (39)$$

iv) when the side cutting edge is removing chip from the surface previously generated by the same part of tool

$$D_4'(p) = F\cos C_s/\cos\eta_c' \quad (40)$$

v) when the end cutting edge removes chip from the surface previously generated by the side cutting edge

$$D_5'(p) = \frac{R[\cos\eta_c' - \sin(\eta_c'+C_s-C_e)]}{\cos\eta_c'\sin(\eta_c'+C_s-C_e)} - \frac{p\cos(\eta_c'+C_s)\cos(C_s-C_e)}{\cos\eta_c'\sin(\eta_c'+C_s-C_e)} + F\cos C_s/\cos\eta_c' \quad (41)$$

vi) when the tool nose removes chip from surface previously cut by the side cutting edge

$$D_6'(p) = [R^2-\{p\cos(\eta_c'+C_s)\}^2]^{1/2} + \frac{F\cos C_s - [p\cos(\eta_c'+C_s)\sin\eta_c' + R]}{\cos\eta_c'} \quad (42)$$

vii) when cutting is done by the end cutting edge of tool against the surface previously cut by the tool nose

$$D_7'(p) = F\cos(\eta_c'+C_s) - [R^2 - p\cos(\eta_c'+C_s) - F\sin(\eta_c'+C_s)\}^2]^{1/2} + \frac{R-p\cos(\eta_c'+C_s)\cos(\eta_c'+C_s-C_e)}{\sin(\eta_c'+C_s-C_e)} \quad (43)$$

viii) when the tool nose is removing chip from the surface previously cut by the same part of the tool

$$D_8'(p) = [R^2-\{p\cos(\eta_c'+C_s)\}^2]^{1/2} - [R^2-\{p\cos(\eta_c'+C_s) - F\sin(\eta_c'+C_s)\}^2]^{1/2} + F\cos(\eta_c'+C_s) \quad (44)$$

Substituting the proper expressions for the undeformed chip thickness and the inner and outer modulation in 32 and 33 and solving 34 the thrust force component of the resultant cutting force is calculated from:

$$F_t = F'\{\cos\beta\sin(\eta_c'+C_s) + (\sin\beta - \cos\beta\tan\alpha_e)\tan\psi\cos(\eta_c'+C_s)\}$$

where

$$\beta = \tan^{-1}F_c'/F_t'$$

$$\alpha_n' = \tan^{-1}(\tan\alpha_n\cos C_s/\cos i - \tan i\sin C_s)$$

$$i' = \tan^{-1}(\tan i\cos C_s + \tan\alpha_n\sin C_s/\cos i)$$

$$\psi = \tan^{-1}(\tan\theta\cos\alpha_e)$$

$$\theta = \cos^{-1}[\{\sin\alpha_e\sin(\eta_c'+C_s)\tan i' + \sin\alpha_e\cos(\eta_c'+C_s)\tan\alpha_n' + \cos\alpha_e\}/\{1+\tan^2 i' + \tan^2\alpha_n'\}^{1/2}]$$

$$F' = [(F_c')^2 + (F_t')^2]^{1/2}$$

## 8. Prediction of the Limiting Depth of Cut

It is known that chatter is caused by the interaction between the directional cutting force and the machine tool structure. It is also known that a major role is played by the thrust force component $F_t$. Therefore for simplicity only this component will be considered. It is practically possible to separate inner modulation effects and outer modulation effects

(4). Therefore the cutting stiffness transfer function will be decomposed as:

$$T_t(j\omega)=F_t/X_t=T_t^i(j\omega)+T_t^o(j\omega) \quad (47)$$

$$T_t^o(j\omega)=\mu e^{-j\epsilon}\,T_t^o \quad (48)$$

$T_t^i(j\omega)$ : Transfer function due to inner modulation alone

$T_t^o(j\omega)$ : Transfer function due to outer modulation alone

For further analysis the flow chart below is convenient.

As a first approximation the machine tool structure will be represented by a single degree of freedom. This is done as follows:

The dynamic characteristics of the machine are determined under actual cutting conditions by recording the random thrust force component $F_t$ and the corresponding minute tool-specimen relative displacement.

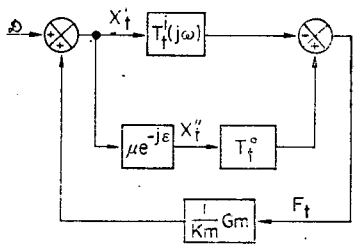


**Fig. 7** The flow chart.

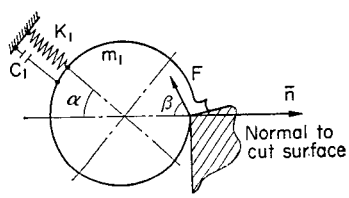


**Fig. 8** Single degree of freedom.

The resulting gain and phase data is used in curve fitting to the stiffness transfer function of a single degree of freedom given by: $H(j\omega)$.

$$H(j\omega)=K_M(1-q^2+2j\,\xi q)$$

$$=\left[\frac{1}{K_M}G_m\right]^{-1} \quad (49)$$

where

$$q=\omega/\omega_n,\ \omega_n^2=K_1/M_1,\ \xi=C_1/2(K_1M_1)^{1/2}$$

$$1/K_M=g_1/K_1,\ g_1=\cos(\alpha_1-\beta_1)\cos\alpha_1$$

Taking only $F_t$ into consideration, $\beta_1=0$ and so $g_1=\cos^2\alpha_1$ The dynamic stiffness transfer functions are illustrated below. It is observed that $T_t(j\omega)$ is a circle whose centre is located in the 3rd quadrant of the complex plane and is slightly below the real axis.

It is observed that as the depth of cut is increased the the radius of $T_t(j\omega)$ increases. We recall that chatter starts to grow when $T_t(j\omega)$ touches $H(j\omega)$. Therefore a computer algorithm for computing the limiting depth of cut may be developed as follows: select the ranges of depth of cut, velocity, frequency, within which the limitiing depths of cut will be determined. With $\mathcal{D}$ and $V$ fixed vary $f$ and search for the coincidence of vectors $\overline{OS}$ and $\overline{OM}$, the cutting velocity $V$, is increased and the search from the starting frequency to end frequency is repeated. This continues until the range of cutting velocity is covered. Next the depth of cut is changed and the above procedure repeated. This is done until the range of depth of cut is also covered. From the data so obtained the asymptotic borderline of stability may be constructed.

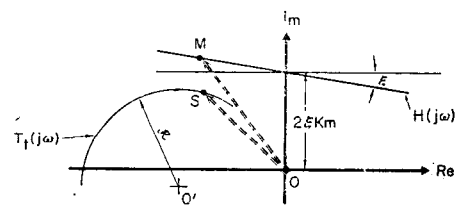


**Fig. 9** $H(\omega)$ and $T_t(\omega)$.

## 9. Experiments

a) Preliminary: Steady state orthogonal cutting experiments are performed with carbon steel, S45C, to obtain the following data:
Main stress of specimen material
$K_c=117.11\,\mathrm{kg/mm^2}$ (50)

Shear stress of the same material

$K_s=77.07\,kg/mm^2$ (51)

Shear angle relation

$\phi_e=0.359+0.025\alpha_n$ (52)

Friction angle relation

$\beta=\exp(1.486\alpha_n-0.44)$ (53)

b) Direct cutting tests: The experimental set-up is illustrated in Fig. 10. An oversize specimen prepared from the same material as that used in a) is held in the lathe to be tested and turned to its final dimensions. Clamping torque of both the specimen and the tool are held constant. The specimen is machined as shown in Fig. 10, thus the depth of cut gradually increases due to the taper. At $\phi$ 74 the thrust force component and the corresponding tool specimen relative displacement are recorded.

Cutting is continued until the onset of chatter is recognized by the chatter sound. The above setting is repeated again so that two such cutting test are carried out. With the data so obtained the average limiting depth of cut is measured as shown in Fig. 10. The recorded signals are processed by using HP 5420A signal analyzer to obtain the transfer function of the machine tool structure. One of the typical transfer functions of the machine tool structure is illustrated in Fig. 11.

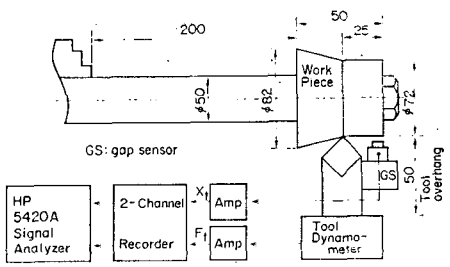


**Fig. 10** A schematic diagram of the experimental set-up.

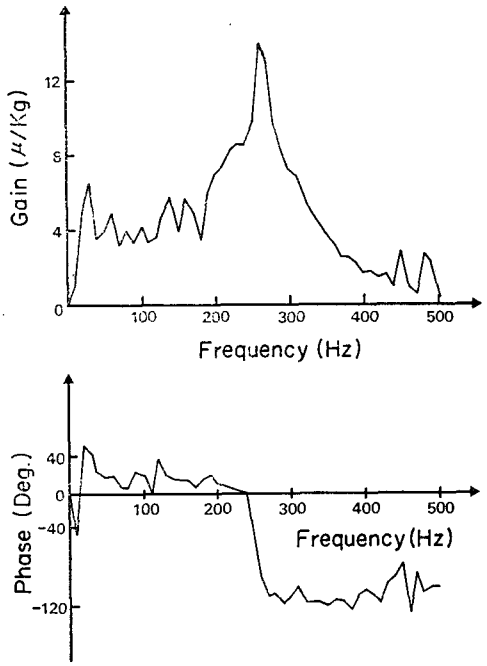


**Fig. 11** Dynamic characteristics of machine tool. Cutting conditions: r.p.m. =290, feed=0.05 mm/rev. tool: p10(0, −7, 7, 45, 45, 0.4)

## 10. Results and Discussions

a) In Fig. 12 it is observed that chip-flow angle predicted by energy method approaches faster the main cutting edge inclination angle than that predicted by Colwell's method. This points out the inaccuracy of colwell's method when the normal rake is different from 0.

b) In Fig. 13 the effect of the side cutting edge angle on chip flow angle is illustrated. For the same cutting conditions and tool geometry chip-flow angle is reduced by increasing the side cutting edge angle of the tool. A reverse effect is observed for an increase in nose radius as shown in Fig. 14.

c) As shown in Fig. 16 comparision of the direct and the indirect test results shows that at relatively high cutting speeds there is good agreement but at lower speeds only an increasing trend in the limiting depth of

cut. The reasons for this are: i) the shear plane model as applied in ref. (5); it is known that this model is not accurate at low cutting speeds. ii) poor modeling of processes at the flank e.g. cutting edge roundness and clearance angle. iii) the difficulty of telling precisely when chatter is caused at low cutting speed. At high speeds a distinctive sound is heard while at low speeds this sound is not so distinct.

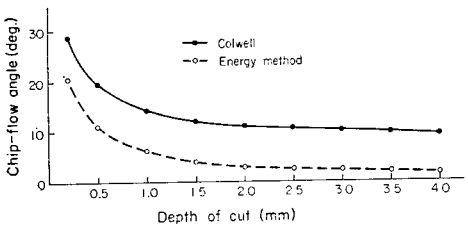


**Fig. 12** Variation of chip flow angle with depth of cut. Tool: p10 (0, −7, 7, 45, 45, 0.4) feed=0.1 mm/rev.

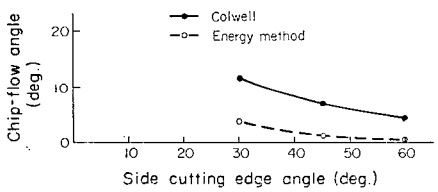


**Fig. 13** Variation of chip flow angle with side c/e angle. feed=0.1 mm/rev. Tool:p 10 (0, −7, 7, 45, var, 0.4).

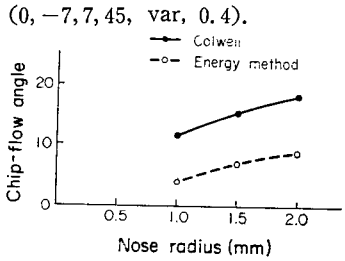


**Fig. 14** Variation of chip flow angle with nose radius. feed=0.1 mm/rev. Tool: p 10 (0, −7, 7, 45, 45, var.).

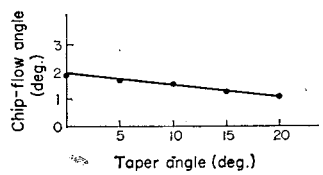


**Fig. 15** Variationof chip-flo angle with taper angle of specimen. Tool: p 10 (0, −7, 7, 5, 45, 0.4) feed=0.1 mm/rev.

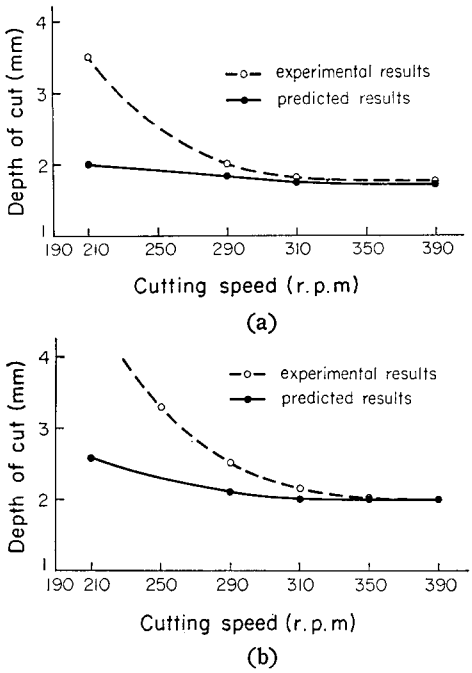


**Fig. 16** Limiting depth of cut. Tool: p 10 (0, −5, 5, 45, 0.4).
(a) feed=0.05 mm/rev.
(b) feed=0.1 mm/rev.

## 11. Conclusion

The theory of cutting dynamics was derived for machine tools with tapered workpieces being cut. Validity of the theory was verified by computing the chatter limits(limiting depth of cut) and comparing the computed limits with the experimentally observed limits.

### Acknowledgements

This work was supported by a financial aid of the 1979 and 1980 Korea Science and Engineering Foundation Grant. The authers wish to thank Prof. T. Sata and Dr. T. Inamura of University of Tokyo for their help in this study.

### References

1. E. Usui and A. Hirota, "Analytical predic-

tion of three dimensional cutting process (Part 1and 2) ASME paper No. 77 WA/P ROD-9, 77WA/PROD-10, 1078.

2. The MTIRA, A Dynamic Performance Test for Lathes, 1971.
3. H.E. Merritt, "Theory of self-excited machine tool chatter", ASME, J. Eng. paper No. 64 WA/PROD-13, 1964.
4. Tlusty, "Analysis of the state of research in cutting dynamics". Annal of the CIRP Vol. 27/2, 1978.
5. M.K. Das and S.A. Tobias, "The relation between static and dynamic cutting of metals". Int. J. MTDR. Vol. 7, 1967.
6. T. Inamura and T. Sata, "Analysis of three dimensional cutting dynamics". Journal of the Faculty of Engineering, the University of Tokyo (B) Vol. XXXIII No. 1975.
7. Jang Moo Lee, "A study on machine tool structural dynamics by digital correlation method". Trans. of KSME, Vol. 5, No. 2., 1981.